A Wideband, Quasi-Isotropic, Ambient RF Energy Harvester Combining UHF-TV and FM

Eui Min Jung ⓘ, *Member, IEEE*, Wang-Sang Lee ⓘ, *Senior Member, IEEE*, Rushi J. Vyas, *Senior Member, IEEE*, and Manos M. Tentzeris ⓘ, *Fellow, IEEE*

Abstract—This letter demonstrates, through real-world field tests, an ambient radio frequency (RF) energy-harvesting system (fabricated on low-cost FR4) capable of harvesting from all surrounding ultrahigh-frequency (UHF) TV and FM towers in all UHF-TV and FM frequencies simultaneously to perpetually power a wireless sensor node. The system achieves −10 dB matching across the entire frequency bands. The UHF-TV portion harvested as much as 231 μW (885 μW for FM). The alignment-free, channel-agnostic nature demonstrates potential for ambient RF harvesting's adaption by users outside of the RF community who are not expected to be familiar with antenna alignment and frequency selection.

Index Terms—Ambient RF energy harvesting, antenna, energy harvester, FM, isotropic, matching, TV, wideband, wireless sensor.

Fig. 1.　Harvester block diagram combining UHF-TV and FM.

I. INTRODUCTION

ENERGY harvesting saves labor costs associated with replacing batteries of wireless sensor nodes (WSNs) and Internet-of-Things (IoT) devices and allows them to be deployed in hard-to-reach places (e.g., hazardous areas, complex structures, sealed systems, etc.) where replacing batteries would be impractical. Radio frequency (RF) harvesting is available day and night [1] and can be implemented in tandem with photovoltaic harvesting to complement each other [2]–[5]. Long wavelengths (sub-GHz) of ultrahigh-frequency (UHF) TV and FM broadcast signals allow less attenuation through mediums and enable appropriately sized antennas to harvest more energy without needing to form arrays [6].

UHF-TV signals are primarily horizontally polarized. This letter combines energy harvested via north–south and east–west polarized UHF-TV antennas as well as a vertically polarized FM antenna (dual-band horizontal antennas require more area) by connecting multiple power management units (PMUs) to one capacitor bank (Fig. 1). The FM portion was detailed in

preceding publications [7], [8]. This letter details the UHF-TV portion (Fig. 2) and presents a combined full UHF-TV and FM band, quasi-isotropic, ambient RF energy harvester.

II. UHF-TV ENERGY HARVESTER ANTENNA DESIGN

Fig. 3 shows simulated and measured gain of the antennas fabricated on MG Chemicals 555 (35 μm copper, 1.6 mm FR4, $\epsilon = 4.2$, and $\delta = 0.015$ at 1 GHz). A triangular sheet dipole with rectangular ends for wider bandwidth is on each front and rear side. The feeds are 50 Ω. The dimensions were exhaustively swept in a full-wave electromagnetic simulation tool (CST Microwave Studio) to balance S_{11} and gain. Front and rear antenna gains combined is 1 or greater across all θ and ϕ, allowing isotropic harvesting, i.e., $G_{\text{front}}(\theta, \phi) + G_{\text{rear}}(\theta, \phi) \geq 1$. If a horizontally polarized wave arrives from the $\phi = 45°$ direction, half of the received power would be contributed by the front antenna and the other half by the rear antenna. These are not one individual antenna with an isotropic gain; such hypothetical antenna does not exist in real life. Fig. 4 shows simulated and measured radiation efficiency. The radiation efficiency is above 85% across the entire UHF-TV band.

Fig. 5 shows simulated and measured S_{11} while the antenna substrate is isolated from the rest of the harvester. The antenna achieves −10 dB matching across the entire UHF-TV band (of the United States) and fractional bandwidth (FBW) as wide as 36%. Fig. 6 shows measured S-parameters while the harvester
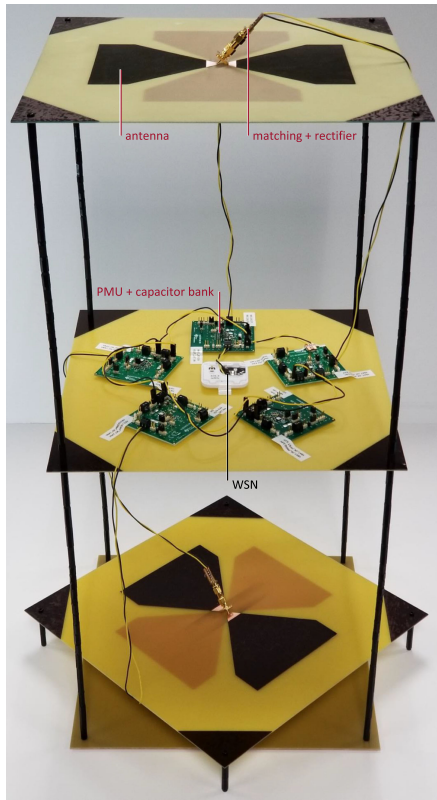
Fig. 2.   UHF-TV harvester. Two pairs of antennas are used, because the matching/rectifying circuits cover upper and lower bands separately.
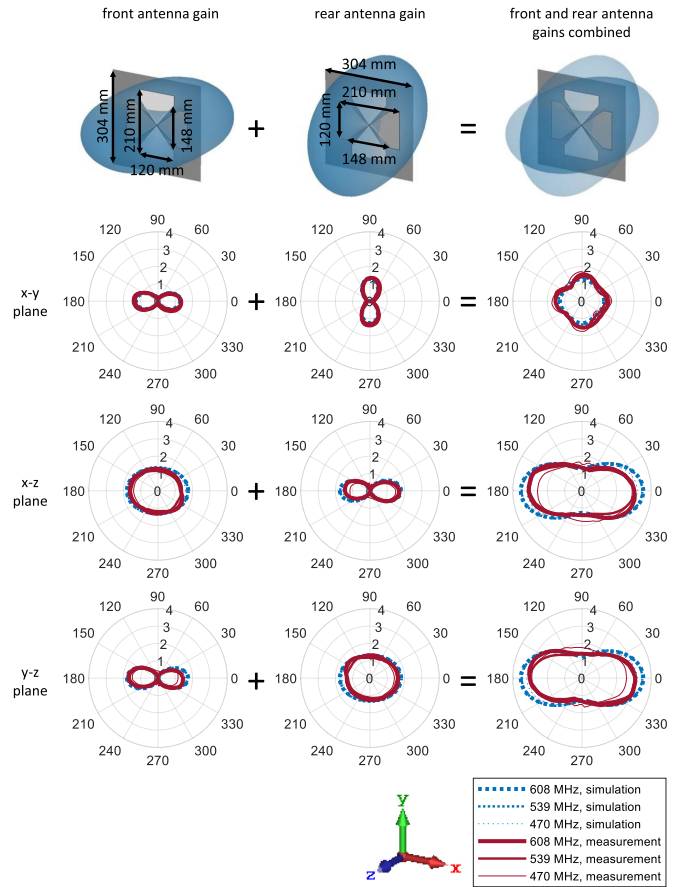

Fig. 3.   Realized gain of the UHF-TV antennas (linear scale, angle in degrees). Front and rear antenna gains combined is 1 or greater across all θ and ϕ.
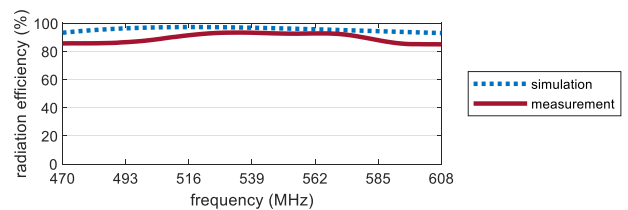

Fig. 4.   Simulated and measured radiation efficiency of the UHF-TV antenna.

is assembled as depicted in Fig. 7 (which shows the combined UHF-TV and FM harvester powering the WSN). The top (port 1) and bottom (port 2) substrate antennas achieve -10 dB matching across the entire UHF-TV band. The substrates are 608 mm apart, separated by a copper-backed PMU/WSN plate, and rotated $45°$ relative to each other around the *z*-axis for isolation (Fig. 2). The TV antennas are horizontally polarized, whereas the FM antenna (port 3) is vertically polarized. The antennas achieve 30 dB isolation among one another across the entire UHF-TV band.

III. MATCHING AND RECTIFYING CIRCUIT DESIGN

Fig. 8 shows schematics of the matching and rectifying circuits. The rectifying circuit was fabricated on MG Chemicals 555. The impedance was measured, component values were exhaustively swept in Keysight Advanced Design System (ADS) to match the impedance, the impedance was measured again after placing the component nearest to the rectifying circuit, and the process was repeated until the component nearest to the antenna was placed. Two matching network stages and one rectifying stage per circuit were used to minimize losses introduced by components, while FR4 was chosen for its low cost and mechanical robustness despite being relatively lossy. The PMU (Texas Instruments BQ25570) was represented by a 3.3 kΩ load. (The PMU has maximum power point tracking.) Fig. 9 shows simulated and measured S_{11}. The two circuits

for the upper and lower half bands together achieve -10 dB matching across the entire UHF-TV band and across all power levels from -20 to 0 dBm. The combined FBWs are 27%, 31%, and 31% for -20, -10, and 0 dBm, respectively. The FBWs for upper and lower band circuits are 14%, 21%, 23% and 17%, 18%, 15%, respectively. Fig. 10 shows measured RF-dc efficiency (η) with varying loads (i.e, compatibility with various loads). Peak RF-dc η occurs at 4.7–5.6 kΩ. Fig. 10 shows RF-dc η across the UHF-TV band at 4.7 kΩ (i.e., compatibility with towers broadcasting in various UHF-TV frequencies). Fig. 11 shows measured RF-dc η and output potential. Note that RF-dc η increasing with input power is a characteristic of Schottky diodes [9], [10]. The PMU requires 100 mV and 5 μW (330 mV and 15 μW for cold-start). Fig. 12 shows measured sensitivity
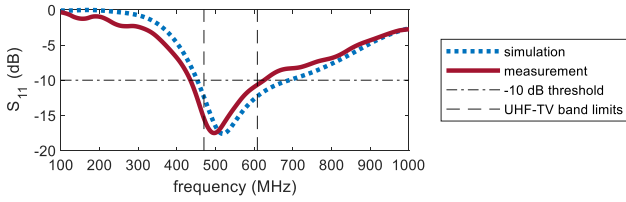
Fig. 5. Simulated and measured S_{11} (isolated antenna). The antenna achieves -10 dB matching across the entire UHF-TV band and FBW as wide as 36%.
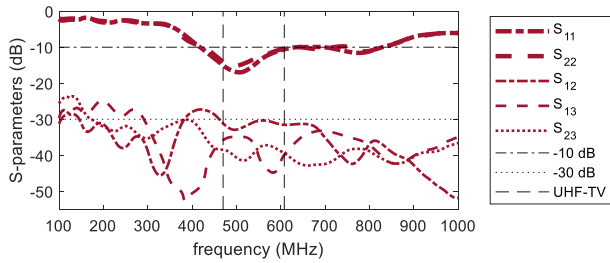

Fig. 6. Measured S-parameters while the harvester is assembled. The top (port 1) and bottom (port 2) substrate antennas achieve -10 dB matching across the entire UHF-TV band. The antennas, including the FM antenna (port 3), achieve 30 dB isolation among one another across the entire UHF-TV band.
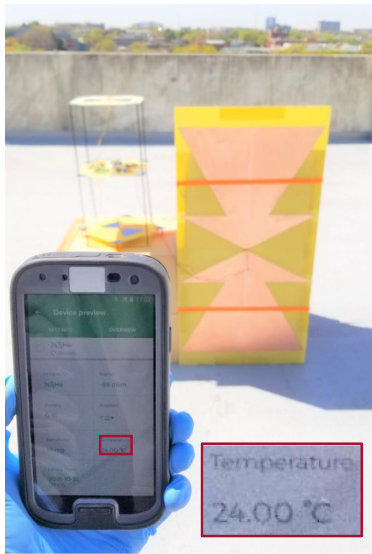

Fig. 7. UHF-TV and FM harvester powering the WSN at the test site.
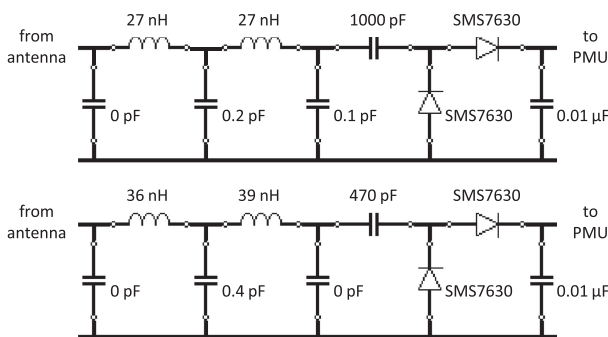

Fig. 8. Matching and rectifying circuits for the upper half (top) and the lower half (bottom) of the UHF-TV band.
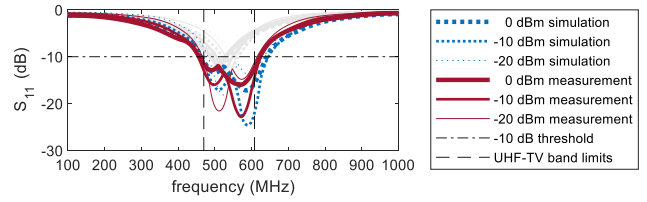

Fig. 9. Simulated and measured S_{11} of the matching and rectifying circuits. The circuits together achieve -10 dB matching across the entire UHF-TV band and across all power levels from -20 to 0 dBm.
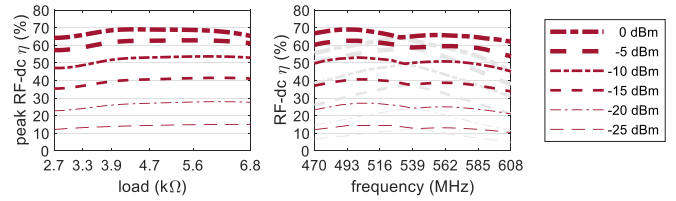
Fig. 10. Measured RF-dc η of the matching and rectifying circuits with varying load (left) and across the UHF-TV band (right).
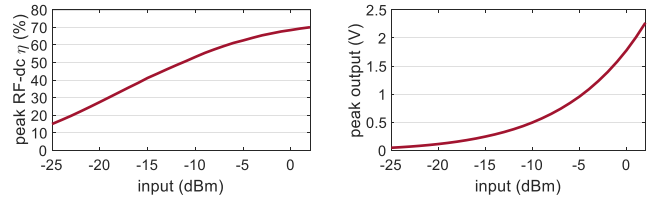
Fig. 11. Measured RF-dc η (left) and output potential (right) of the matching and rectifying circuits. The PMU requires 100 mV (330 mV for cold-start).
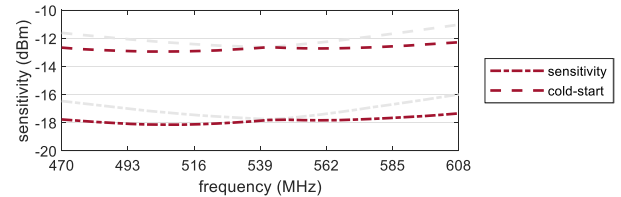
Fig. 12. Measured sensitivity and cold-start sensitivity of the matching and rectifying circuits. As low as -18 and -13 dBm are achieved, respectively.

and cold-start sensitivity. As low as -18 and -13 dBm are achieved, respectively. Single-tone RF input was used for these measurements. Multitone RF inputs such as UHF-TV get added in time domain and yield higher output potential.

IV. SYSTEM DEMONSTRATION AND COMPARISON TO RELATED WORK

A. System Demonstration

Fig. 13 shows the power spectrum measured using the harvester antennas at the test site (33.7759, -84.3898). The power density was measured to be 1.2 mW/m^2 for the UHF-TV band (3.1 mW/m^2 for the FM band). The highest contribution comes from channel 18 for UHF-TV (91.1 MHz for FM). Fig. 14

TABLE I
COMPARISON OF AMBIENT RF ENERGY-HARVESTING WORK

|	antenna radiation pattern (physical area)	-10 dB FBW	RF-dc η	harvested power	final load
[11]	unidirectional ($0.39\,\lambda^2$)	2 % @ -15 dBm	14 % @ -20 dBm	49 μW @ NA	WSN
[12]	omnidirectional (NA)	NA	0.8 % @ -20 dBm	0.3 μW @ 0.2 km	capacitor
[13]	unidirectional ($2.1\,\lambda^2$)	2 % @ -20 dBm	28 % @ -20 dBm	80 μW @ NA	resistor
[14]	unidirectional ($0.70\,\lambda^2$)	3 % @ -20 dBm	30 % @ -20 dBm	NA	open
[15]	unidirectional ($0.09\,\lambda^2$)	33 % @ -15 dBm	15 % @ -20 dBm	15 μW @ 0.05 km	resistor
[16]	bidirectional ($0.25\,\lambda^2$)	9 % @ -10 dBm	32 % @ -20 dBm	6.2 μW @ NA	resistor
[17]	omnidirectional ($0.012\,\lambda^2$)	4 % @ -10 dBm	5 % @ -20 dBm	NA @ 6.3 km	WSN
[18]	unidirectional ($0.20\,\lambda^2$)	2 % @ -15 dBm	7 % @ -15 dBm	17 μW @ 6.3 km	μ-controller
[19]	bidirectional (NA)	7 % @ -20 dBm	NA	3.6 μW @ NA	LED
[20]	unidirectional (NA)	NA	NA	NA @ 4.2 km	WSN
[21], [22]	unidirectional (NA)	NA	25 % @ -5 dBm	60 μW @ 4.1 km	sensor
[23], [24]	bidirectional ($0.17\,\lambda^2$)	32 % @ -20 dBm	30 % @ -20 dBm	67 μW @ NA	resistor
this work	quasi-isotropic ($0.30\,\lambda^2$)	27 % @ -20 dBm	28 % @ -20 dBm	231 μW @ 5.83 km	WSN
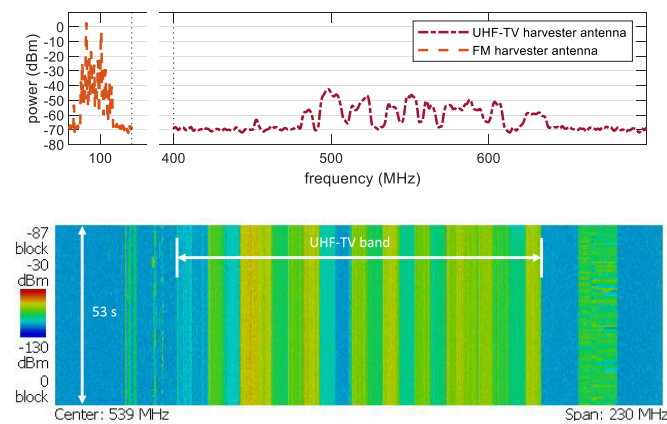
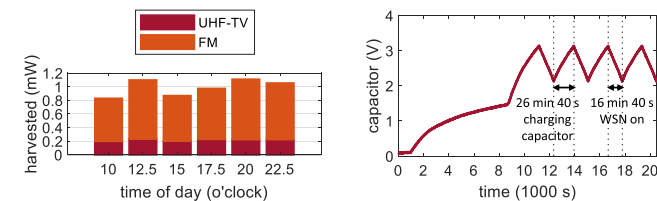Fig. 13. Spectrum measured using the harvester antennas at the test site.

Fig. 14. Power harvested throughout a day at the test site (left) and UHF-TV harvester charge cycle powering the WSN (right). As much as 231 and 885 μW were harvested from UHF-TV and FM bands, respectively.

shows the power harvested throughout a day. The UHF-TV portion consistently harvested 200 μW or higher, reaching as high as 231 μW. Fig. 14 shows the UHF-TV harvester's charge cycle powering the WSN. The WSN (Kontakt.io S18-3) was powered for 16 min 40 s after every 26 min 40 s of charging. Measured RF-dc η was 40%. Capacitance (three parallel Seiko CPH3225A) was chosen to provide enough current to turn on the WSN. Charge cycle measurement does not exist for combined UHF-TV and FM harvesting, because the FM harvester, even on its own, can power the WSN without periodically shutting down [7], [8].

B. Comparison to Related Work

Table I compares ambient RF energy harvesting work [11]–[24]. The frequency band showing the best performance was selected for each work. Only this work is capable of harvesting from all directions using its quasi-isotropic antenna setup. The antenna of this work has competitive size while achieving wide bandwidth. (Wider bandwidth requires larger antenna size [6].) Only this and one other work achieve double-digit -10 dB FBW at -20 dBm. The RF-dc η of this work is among the leaders, again, while achieving wide bandwidth. (Lower loss is easier to achieve with narrow-band matching.) No other work was able to harvest triple-digits of μW. This work is among the few that demonstrate powering a WSN. WSN/IoT devices have power and potential requirements for cold-start and for staying on. Without these constraints, wide bandwidth and high efficiency are easier to achieve and thus have diminished significance. Systems that do not demonstrate powering such load may not be capable of providing useful function.

Only this letter allows harvesting from all surrounding towers simultaneously, whereas the others focus on harvesting from single sources at specific frequencies using directional antennas. Requiring careful alignment with calibration equipment prevents ambient RF energy harvesting from being adapted outside of the RF community. It is also impractical when deploying in mass scale, when towers are visually obstructed, or when it is unknown which tower provides the most power to a given location [25]. Only this work addresses these issues.

V. CONCLUSION

This work demonstrates an ambient RF energy-harvesting system (fabricated on low-cost FR4) capable of harvesting from all surrounding UHF-TV and FM towers in all UHF-TV and FM frequencies simultaneously to perpetually power a WSN. Front and rear antenna gains combined is 1 or greater across all θ and ϕ, allowing isotropic harvesting. The system achieves -10 dB matching across the entire frequency bands. The system is as sensitive as -18 dBm. The UHF-TV portion harvested as much as 231 μW (885 μW for FM). The alignment-free, channel-agnostic nature of this work demonstrates the potential for widespread adaption of ambient RF energy harvesting.

REFERENCES

[1] S. Kim *et al.*, "Ambient RF energy-harvesting technologies for self-sustainable standalone wireless sensor platforms," *Proc. IEEE*, vol. 102, no. 11, pp. 1649–1666, Nov. 2014.

[2] A. Collado and A. Georgiadis, "Conformal hybrid solar and electromagnetic (EM) energy harvesting rectenna," *IEEE Trans. Circuits Syst. Reg. Papers*, vol. 60, no. 8, pp. 2225–2234, Aug. 2013.

[3] K. Niotaki, A. Collado, A. Georgiadis, S. Kim, and M. M. Tentzeris, "Solar/electromagnetic energy harvesting and wireless power transmission," *Proc. IEEE*, vol. 102, no. 11, pp. 1712–1722, Nov. 2014.

[4] J. Bito, R. Bahr, J. G. Hester, S. A. Nauroze, A. Georgiadis, and M. M. Tentzeris, "A novel solar and electromagnetic energy harvesting system with a 3-D printed package for energy efficient Internet-of-Things wireless sensors," *IEEE Trans. Microw. Theory Techn.*, vol. 65, no. 5, pp. 1831–1842, May 2017.

[5] Y. Zhang, S. Shen, C. Y. Chiu, and R. Murch, "Hybrid RF-solar energy harvesting systems utilizing transparent multiport micromeshed antennas," *IEEE Trans. Microw. Theory Techn.*, vol. 67, no. 11, pp. 4534–4546, Nov. 2019.

[6] L. J. Chu, "Physical limitations of omni-directional antenna," *J. Appl. Phys.*, vol. 19, no. 12, pp. 1163–1175, 1948.

[7] E. M. Jung *et al.*, "A wideband, quasi-isotropic, kilometer-range FM energy harvester for perpetual IoT," *IEEE Microw. Wireless Compon. Lett.*, vol. 30, no. 2, pp. 201–204, Feb. 2020.

[8] Y. Cui, E. M. Jung, A. O. Adeyeye, C. Lynch, X. He, and M. Tentzeris, "Additively manufactured RF devices for 5G, IoT, RFID, WSN, and smart city applications," *Int. J. High Speed Electron. Syst.*, vol. 29, no. 01n04, 2020, Art. no. 2040016.

[9] B. R. Marshall, M. M. Morys, and G. D. Durgin, "Parametric analysis and design guidelines of RF-to-DC Dickson charge pumps for RFID energy harvesting," in *Proc. IEEE Int. Conf. RFID*, 2015, pp. 32–39.

[10] C. H. P. Lorenz *et al.*, "Breaking the efficiency barrier for ambient microwave power harvesting with heterojunction backward tunnel diodes," *IEEE Microw. Wireless Compon. Lett.*, vol. 63, no. 12, pp. 4544–4555, Dec. 2015.

[11] U. Muncuk, K. Alemdar, J. D. Sarode, and K. R. Chowdhury, "Multiband ambient RF energy harvesting circuit design for enabling batteryless sensors and IoT," *IEEE Internet Things J.*, vol. 5, no. 4, pp. 2700–2714, Aug. 2018.

[12] S. Kitazawa, H. Ban, and K. Kobayashi, "Energy harvesting from ambient RF sources," in *Proc. IEEE MTT-S Int. Microw. Workshop Ser. Innov. Wireless Power Transmiss.: Technol., Syst., Appl.*, 2012, pp. 39–42.

[13] S. Shen, Y. Zhang, C. Chiu, and R. Murch, "A triple-band high-gain multibeam ambient RF energy harvesting system utilizing hybrid combining," *IEEE Trans. Ind. Electron.*, vol. 67, no. 11, pp. 9215–9226, Nov. 2020.

[14] H. Sun, Y. Guo, M. He, and Z. Zhong, "A dual-band rectenna using broadband Yagi antenna array for ambient RF power harvesting," *IEEE Antennas Wireless Propag. Lett.*, vol. 12, pp. 918–921, 2013.

[15] V. Kuhn, C. Lahuec, F. Seguin, and C. Person, "A multi-band stacked RF energy harvester with RF-to-DC efficiency up to 84%," *IEEE Trans. Microw. Theory Techn.*, vol. 63, no. 5, pp. 1768–1778, May 2015.

[16] C. Song, Y. Huang, J. Zhou, J. Zhang, S. Yuan, and P. Carter, "A high-efficiency broadband rectenna for ambient wireless energy harvesting," *IEEE Trans. Antennas Propag.*, vol. 63, no. 8, pp. 3486–3495, Aug. 2015.

[17] R. Shigeta *et al.*, "Ambient RF energy harvesting sensor device with capacitor-leakage-aware duty cycle control," *IEEE Sensors J.*, vol. 13, no. 8, pp. 2973–2983, Aug. 2013.

[18] R. J. Vyas, B. B. Cook, Y. Kawahara, and M. M. Tentzeris, "E-WEHP: A batteryless embedded sensor-platform wirelessly powered from ambient digital-TV signals," *IEEE Trans. Microw. Theory Techn.*, vol. 61, no. 6, pp. 2491–2505, Jun. 2013.

[19] M. Piñuela, P. D. Mitcheson, and S. Lucyszyn, "Ambient RF energy harvesting in urban and semi-urban environments," *IEEE Trans. Microw. Theory Techn.*, vol. 61, no. 7, pp. 2715–2726, Jul. 2013.

[20] A. N. Parks, A. P. Sample, Y. Zhao, and J. R. Smith, "A wireless sensing platform utilizing ambient RF energy," in *Proc. IEEE Topical Conf. Biomed. Wireless Technol., Netw., Sens. Syst.*, 2013, pp. 154–156.

[21] A. Sample and J. R. Smith, "Experimental results with two wireless power transfer systems," in *Proc. IEEE Radio Wireless Symp.*, 2009, pp. 16–18.

[22] A. P. Sample, D. J. Yeager, P. S. Powledge, A. V. Mamishev, and J. R. Smith, "Design of an RFID-based battery-free programmable sensing platform," *IEEE Trans. Instrum. Meas.*, vol. 57, no. 11, pp. 2608–2615, Nov. 2008.

[23] C. Song, Y. Huang, J. Zhou, and P. Carter, "Improved ultrawideband rectennas using hybrid resistance compression technique," *IEEE Trans. Antennas Propag.*, vol. 65, no. 4, pp. 2057–2062, Apr. 2017.

[24] C. Song *et al.*, "A novel six-band dual CP rectenna using improved impedance matching technique for ambient RF energy harvesting," *IEEE Trans. Antennas Propag.*, vol. 64, no. 7, pp. 3160–3171, Jul. 2016.

[25] Y. Hu, S. Sun, H. Xu, and H. Sun, "Grid-array rectenna with wide angle coverage for effectively harvesting RF energy of low power density," *IEEE Trans. Microw. Theory Techn.*, vol. 67, no. 1, pp. 402–413, Jan. 2019.